Wear Behavior of Alkali-Treated Sorghum Straw Fiber Reinforced Polyvinyl Chloride Composites in Corrosive Water Conditions

Liangpeng Jiang,[a] Chunxia He,[a,*] Jingjing Fu,[b] and Xiaolin Li [a]

The application of wood-plastic composites is growing rapidly in the fields of corrosion and aging. The present study investigated the effect of alkali-treated (with NaOH concentrations of 0.5, 2.5, 4.5, and 6.5%) sorghum straw (SS) fiber on the wear resistance of polyvinyl chloride (PVC) composites under simulated seawater and acid rain conditions. The results showed that the wear resistance of the SS/PVC composites was noticeably improved by the addition of the alkali-treated SS fiber. SS fiber treated with 4.5% NaOH showed low polarity and hydrophilicity with high crystallinity and improved mechanical properties, which endowed the SS/PVC composites with high interfacial bonding and wear resistance. Exposure to simulated seawater and acid rain resulted in the deterioration of physical (including water repellency and hardness), mechanical, thermal, and wear-resistance properties of the composites; the wear mechanism of the SS/PVC composites after corrosion for 12 days was mainly abrasive wear.

Keywords: Alkali treatment; Sorghum straw; Seawater; Acid rain; Wear

*Contact information: a: College of Engineering, Nanjing Agricultural University, Nanjing 210031, China; b: Nanjing Research Institute for Agricultural Mechanization, Ministry of Agriculture, Nanjing 210014, China; * Corresponding author: chunxiahe@hotmail.com*

INTRODUCTION

With the high global energy demand and increasing environmental awareness, natural fiber polymer composites (NFPCs) have received widespread attention due to their advantageous economic and ecological properties. Various aspects of industrial production and manufacturing, such as cladding and decking, can be produced using these NFPCs (Yang *et al.* 2015; Friedrich and Luible 2016). There are many situations where NFPCs are exposed to tribological loading conditions (Bajpai *et al.* 2013). Therefore, understanding the tribological behavior, as well as the mechanical properties of NFPCs are of equal importance (Yousif *et al.* 2010a).

Recently, tribological analysis of polymer composites based on natural fibers such as jute (Chand and Dwivedi 2006), cotton (Hashmi *et al.* 2007), sisal (Xin *et al.* 2007; Chand and Dwivedi 2010), oil palm (Yousif and El-Tayeb 2008), sugarcane (El-Tayeb 2008), kenaf (Chin and Yousif 2009), betelnut (Singh Gill and Yousif 2009; Nirmal *et al.* 2010), and bamboo (Nirmal *et al.* 2012) have been performed. However, there have been few studies on the effect of aging in corrosive solutions (such as sea water and acid rain) on the wear behavior of the NFPCs (Yousif and Nirmal 2011; Jiang *et al.* 2017a, b). Hence, further studies in this field should measure the impact of aging on the wear characteristics of NFPCs. In addition, the most influential aspect in the design of NFPCs subjected to tribological loading is the interfacial bonding of the fiber with the matrix (Shalwan and Yousif 2013).

NaOH treatment is the most effective treatment method to enhance the interfacial bonding of natural fibers with a polymer matrix; other techniques exhibited either no effect or deterioration of the fiber strength (Alawar *et al.* 2009; Yousif *et al.* 2010b; Phuong *et al.* 2010; Saha *et al.* 2010). Natural fiber treated with 6% NaOH was used to prepare fiber reinforced polymer composites (T-NFPCs), and the product showed a less specific wear rate in comparison to the untreated composites (U-NFPCs). The favorable performance was attributed to high interfacial bonding of natural fibers with polymer matrix preventing fiber pullout during the sliding (Yousif and EI-Tayeb 2008; Singh Gill and Yousif 2009).

This study explored the aging effects of alkali-treated sorghum straw fiber-reinforced polyvinyl chloride composites under simulated seawater and acid rain conditions. These experiments elucidated the wear behaviors of NFPCs in outdoor applications.

EXPERIMENTAL

Materials

Sorghum straw (SS) was sourced from a local farmland in Nanjing, China. SG-5 PVC was purchased from Tianye Group Co., Ltd., Xinjiang, China. Silane coupling agent KH-550 was purchased from Chuangshi Chemical Additives Co., Ltd., Nanjing, China. The 603 non-toxic Ca/Zn composite stabilizer and H-108 PE wax were purchased from Wenhua Chemical Pigment Co., Ltd., Shanghai, China.

Fiber and Sample Preparation

The air-dried SS was crushed, ground, and filtered with a 100-mesh screen (149 μm pore size). Selected SS fibers were soaked in 0.5, 2.5, 4.5, and 6.5% NaOH at 100 °C for 1 h (solid-liquid ratio = 1: 2). The treated fibers were separated from the liquid by filtration and washed with deionized water until the rinsed solution became neutral. The rinsed fibers were then dried at 90 °C for 24 h in a DHG-9140A electro-thermostatic drum-wind drying oven (Dongmai Scientific Instrument Co., Ltd., Nanjing, China).

The KH-550 (3 wt% of SS fiber) was dissolved in absolute ethanol, and the volume ratio of KH-550 to absolute ethanol was 1:5. The diluent was sprayed evenly on the alkali-treated fiber, and the fiber was subsequently allowed to air-dry for 12 h followed by oven-drying at 90 °C for 12 h.

Based on the pre-experiment data, the silane-treated fiber, PVC, stabilizer, and PE wax (mass ratio = 100: 100: 8: 5, respectively) were mixed in a SBH-5L 3D linkage mixer (Xinbao Mechanical and Electrical Industry Co., Ltd., Nanjing, China), followed by melt-blending in a RM200C conical twin-screw extruder (Hapro Electric Technology Co., Ltd., Harbin, China). The corresponding temperatures of the extruder from hopper to die zone were controlled at 150, 155, 160, and 165 °C, respectively, and the rotational speed of the screw was 20 rpm. The cross-section dimensions of the extruded samples were 10 mm wide and 7 mm thick. The solidified samples were cut into lengths of 100 mm for further tests.

Immersion Corrosion of the SS/PVC Composites

Based on previous work (Jiang *et al.* 2017b), alternate simulated sea water (salinity 3.5%, temperature 55 °C, corrosion period 2 days) and acid rain (pH 2.5, temperature 55 °C, corrosion period 2 days) conditions degrade the wear resistance of the SS/PVC

composites (simulating a real outdoor environment with acid rain near the sea during a hot summer). To form the simulated sea water, NaCl (CP, wt% ≥ 99.5) was added to deionized water for a final salinity of 3.5%. A molar ratio of 5:1 (*i.e.*, SO_4^{2-} : NO_3^-) was used to configure the acid mother liquor by mixing H_2SO_4 (purity 98%) and HNO_3 (purity 68%). The acid mother liquor was then diluted with deionized water to pH 2.5, forming the simulated acid rain (Jiang *et al.* 2017a).

The samples were placed in beakers filled with the corrosive solution. The beakers were sealed with film and placed in a constant temperature water-bath in a HH-600 thermostatic water tank (Baidian Instrument Equipment Co., Ltd., Shanghai, China). This test was comprised of three cycles, each composed of 2 steps: (a) first immersing in the simulated sea water at 55 ± 1 °C for 2 d and (b) then immersing in the simulated acid rain at 55 ±1 °C for 2 d. At the end of each cycle (*i.e.*, 4 d), the samples were removed from the solution and left to air-dry until reaching a constant mass (defined by mass variation of less than 1% in a period of 24 h). After air-drying, the samples were stored for further characterization analysis.

Characterization

Physicochemical and mechanical properties of the SS fiber

Fourier transform infrared (FTIR) spectra were obtained using a Nicolet iS10 FTIR spectrometer (Thermo Fisher Scientific Co., Ltd., Shanghai, China) operating at a resolution of 4 cm^{-1} in the range of 400 to 4000 cm^{-1}. The results were averages of 16 scans.

X-ray diffraction (XRD) spectra were obtained using a X'Pert PRO X-ray diffractometer (PANalytical B.V., Almelo, Netherlands, Cu-Kα radiation, λ = 0.15406 Å) operating at 40 KV and 40 mA in the 2θ range of 0 to 90° and a scan rate of 0.33 °·min^{-1}. The crystallinity index (CrI) was calculated using Eq. 1 (Abdul *et al.* 2016),

$$CrI = \left[1 - (I_{am} / I_{002})\right] \times 100 \quad (1)$$

where I_{002} is the intensity of the crystalline phase peak at 2θ = 22.5°, and I_{am} is the intensity of the amorphous phase peak at 2θ = 18°.

The tensile strength and modulus tests of un-crushed raw straw were performed through a CMT6104 electronic universal testing machine (MTS Industrial Systems Co., Ltd., Shanghai, China) according to the Chinese standard GB/T 35378 (2017). For each test, a crosshead speed of 2 mm·min^{-1} was employed, maintaining a gauge length of 30 mm.

Physico-mechanical properties of the SS/PVC composites

The water and moisture absorption (that is, *WA* and *MA*) tests were performed in accordance with the Chinese standard GB/T 17657 (2013) and GB/T 20312 (2006), respectively. Before the test, the samples were oven-dried at 90 °C for 12 h. Subsequently, the samples for the *WA* tests were immersed in deionized water at 23 ± 1 °C for 24 h in a HH-600 thermostatic water tank, and the samples for the *MA* tests were subjected to 90% relative humidity at 23 ± 0.5 °C for 48 h in a HPX-160BSH-III temperature humidity incubator (CIMO Medical Instrument Manufacturing Co., Ltd., Shanghai, China). The *WA* and *MA* values were calculated based on the weight percent gains after removing excess water on the exterior surface.

The hardness tests were performed in accordance with the Chinese standard GB/T 3398.1 (2008). Using a XHR-150 Plastics Rockwell hardness tester (Lianer Testing Equipment Co., Ltd., Shanghai, China) with a scale of R, the indenter diameter was

determined as 12.7 mm. The loading and unloading times were both 15 s, and a load of 60 kg was applied for a period of 5 s.

The compressive, tensile, and flexural strength tests were performed in accordance with the Chinese standards GB/T 1041 (1992), GB/T 1040.1 (2006), and GB/T 9341 (2008), respectively. Using the CMT6104 electronic universal testing machine, the loading speed was 2 mm·min^{-1} in each case.

The data of physical-mechanical properties are the average value of 5 replicate samples under room temperature condition (25 ± 1 °C).

Wear tests of the SS/PVC composites

Wear tests were performed with a M-2000A wear tester (Xuanhua Kehua Testing Machine Manufacturing Co., Ltd., Zhangjiakou, China) using a ring-on-block configuration under dry (air) sliding conditions (room temperature of 25 ± 1 °C). A quench-hardened 45# steel ring (outer diameter 40 mm, surface hardness 40-45 HRC, and surface roughness (R_a) 0.08-0.12 μm) was chosen as a counterpart. The rotating ring slid on the block sample (6 × 7 × 30 mm^3) with a normal load of 100 N, a sliding velocity of 200 rpm, and a sliding time of 120 min. Prior to the wear test, each sample was cleaned with absolute ethanol and then dried in air. Each test was performed in triplicate to assure the reproducibility of the results.

The average friction coefficient (μ) was calculated using the wear tester. The specific wear rate (W_S) was calculated using Eq. 2 (Jeamtrakull *et al.* 2012). ΔM is the weight loss (mg), which was measured by a FA1004 electronic analytical balance (Hengping Scientific Instrument Co., Ltd., Shanghai, China) with an accuracy of 0.1 mg. ρ is the sample density (g·cm^{-3}), which was measured by a DH-300 direct-reading electronic densimeter (Dahometer Instrument Co., Ltd., Dongguan, China). L is the sliding distance (m) and F is the normal load (N).

$$W_S = \frac{\Delta M}{LF\rho} \quad (2)$$

Thermogravimetric and morphological analysis of the SS/PVC composites

Thermogravimetric (TG) analyses were performed using a STA 449 F3 synchronized thermal analyzer (NETZSCH Scientific Instrument Trading Co., Ltd., Selb, Germany) under an argon atmosphere. Samples of 5 to 10 mg were heated from 30 to 800 °C at a heating rate of 20 °C·min^{-1} under flow rates of 20 and 60 mL·min^{-1} for the shielding and sweep gases, respectively.

The morphological analyses were performed using a S-4800 scanning electron microscope (SEM; Hitachi Ltd., Tokyo, Japan). Prior to the SEM analyses, the surfaces of the samples were coated with gold using an E-1010 ion sputter coater.

RESULTS AND DISCUSSION

Physicochemical and Mechanical Properties of the SS Fiber

The FTIR spectra of the untreated and alkali-treated SS fiber are shown in Fig. 1. The strong and broad absorption peak at the range of 3500 to 3300 cm^{-1} arises from the O-H stretching vibration of hydroxyl groups, and was found to decrease with increasing NaOH concentration. This result indicated that alkali treatment reduced the polarity and

hydrophilicity of the SS fiber (Oushabi *et al.* 2017). Similarly, intensity weakening of the absorbance peaks was observed for the 2918, 1635, 1383, and 1053 cm^{-1} peaks. In addition, the peaks at 1740 and 1248 cm^{-1} disappeared almost completely after alkali treatment, indicating that alkali treatment removed functional groups related to hemicellulose, lignin, or pectin in the SS fiber (Cai *et al.* 2015; Krishnaiah *et al.* 2017).

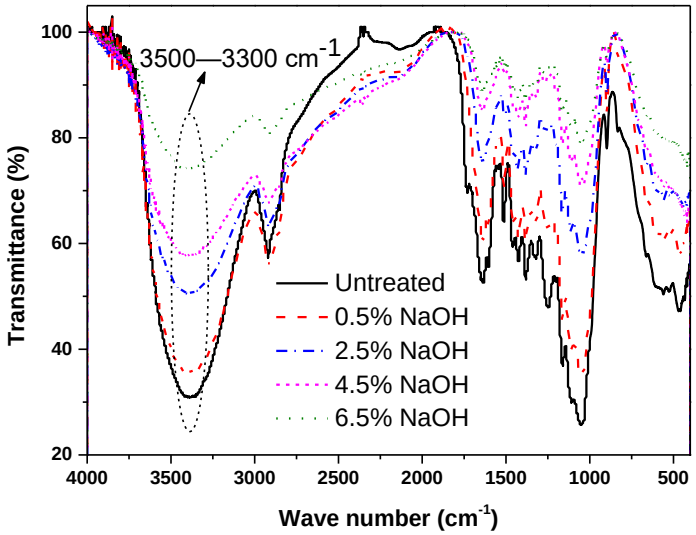

Fig. 1. FTIR spectra of the untreated and alkali-treated SS fiber

For composite application, plant fibers with high crystallinity are required, since the crystallinity correlates with fiber strength and stiffness (Cai *et al.* 2016). The XRD spectra of the untreated and alkali-treated SS fiber are shown in Fig. 2. The crystallinity index of the untreated, 0.5, 2.5, 4.5, and 6.5% alkali-treated SS fibers were 53.5, 57.3, 59.3, 66.1, and 65.3%, respectively. The maximum crystallinity was observed with the 4.5% NaOH treatment, which can be explained by the increased removal of non-cellulosic material (hemicelluloses, lignin and pectin). However, at a higher NaOH concentration (6.5%), the strong alkali solution attacks the main structural components of the SS fiber, resulting in a loss of conformation and crystallinity (Oudiani *et al.* 2011).

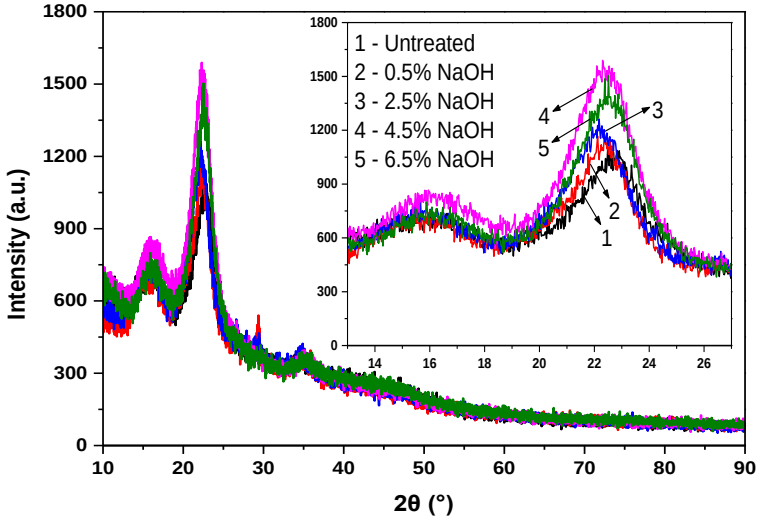

Fig. 2. XRD spectra of the untreated and alkali-treated SS fiber

The tensile strength and modulus of the untreated and alkali-treated raw SS are shown in Fig. 3. Compared with raw SS, the tensile strength and modulus were improved when mild alkali treatment was applied. This enhancement can be explained by the removal of a large amount of hemicelluloses, lignin, and other impurities, which facilitates the rearrangement of fibrils along the direction of extension deformation, resulting in higher tensile strength and modulus. The optimum tensile strength and modulus were observed with the 4.5% NaOH treatment reaching the values of 76.5 MPa and 4.2 GPa, respectively. These values equated to an increase of 31.8% and 27.7%, respectively, compared with the untreated raw SS. However, this trend was reversed when the NaOH concentration was increased to 6.5% due to the strong alkali employed in the treatment, which attacks the main structural components of the SS fiber.

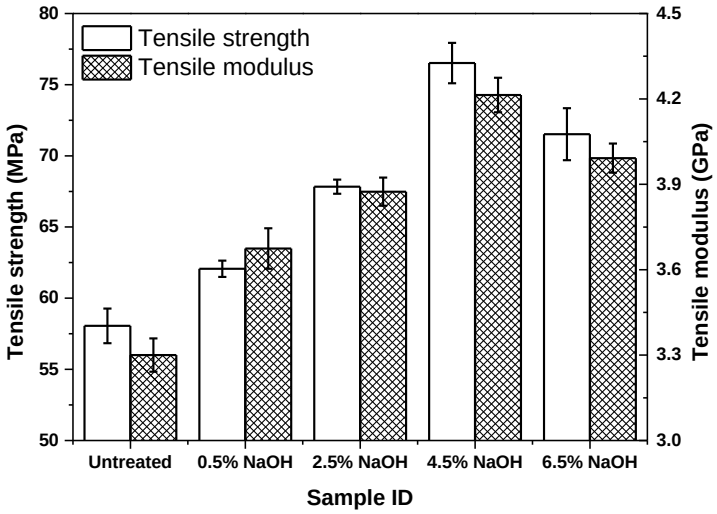

Fig. 3. Tensile strength and modulus of the untreated and alkali-treated raw SS

Water and Moisture Absorption Analysis of the SS/PVC Composites

The 24 h water and 48 h moisture absorption of the wood-plastic composites (WPCs) can indirectly indicate changes in interfacial bonding. Better interfacial bonding indicates increased fiber encapsulation by the matrix, which creates a barrier against the water (or moisture) and results in slow swelling and weight gain for the WPCs (Matuana *et al.* 2011). Overall, for the same corrosion cycle, all alkali-treated SS/PVC composites showed reduced 24 h *WA* and 48 h *MA* values, and 6.5% alkali-treated SS fiber-reinforced PVC (6.5ASRP) had the best water and moisture resistance (6.5ASRP > 4.5% alkali-treated SS fiber-reinforced PVC (4.5ASRP) > 2.5% alkali-treated SS fiber-reinforced PVC (2.5ASRP) > 0.5% alkali-treated SS fiber-reinforced PVC (0.5ASRP) > untreated SS fiber-reinforced PVC (USRP)), as shown in Fig. 4. This result was expected, as the 6.5% alkali-treated SS fiber was more compatible with the weakly-polar PVC matrix than the other fibers due to lack of polar and hydrophilic components (such as -OH) in the fiber, which slowed water and moisture absorption. In addition, the SS/PVC composites had higher 24 h *WA* and 48 h *MA* values as the corrosion cycle progressed, which could be attributed to the alternating corrosion conditions accelerating the formation of micro-cracks at the two-phase interfaces. After water enters the interface through these micro-cracks, it leads to swelling and weight gain of fiber. Based on the 24 h *WA* and 48 h *MA* data, 6.5ASRP had the best interfacial bonding quality, followed by the 4.5ASRP, 2.5ASRP, 0.5ASRP, and USRP composites. Further examination of the micro-cracks in the test samples is explored in next section.

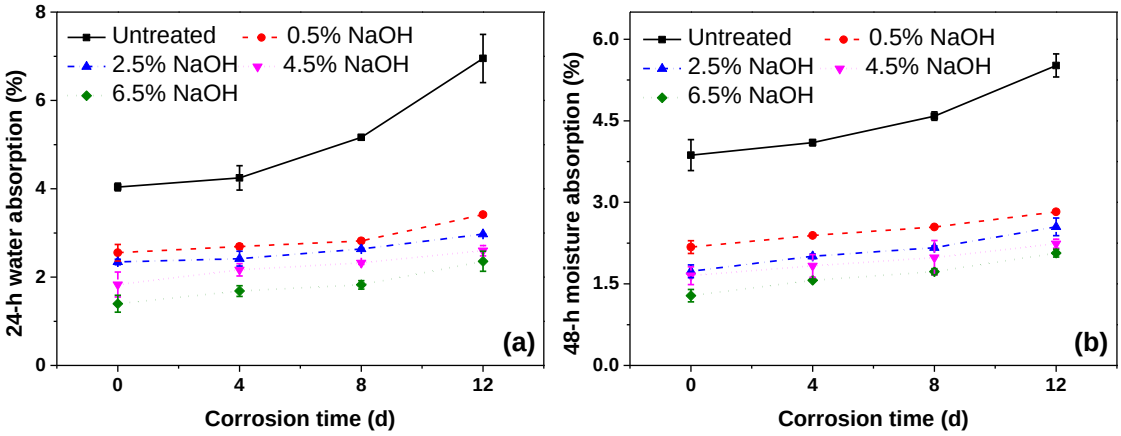

Fig. 4. 24 h water and 48 h moisture absorption of the SS/PVC composites

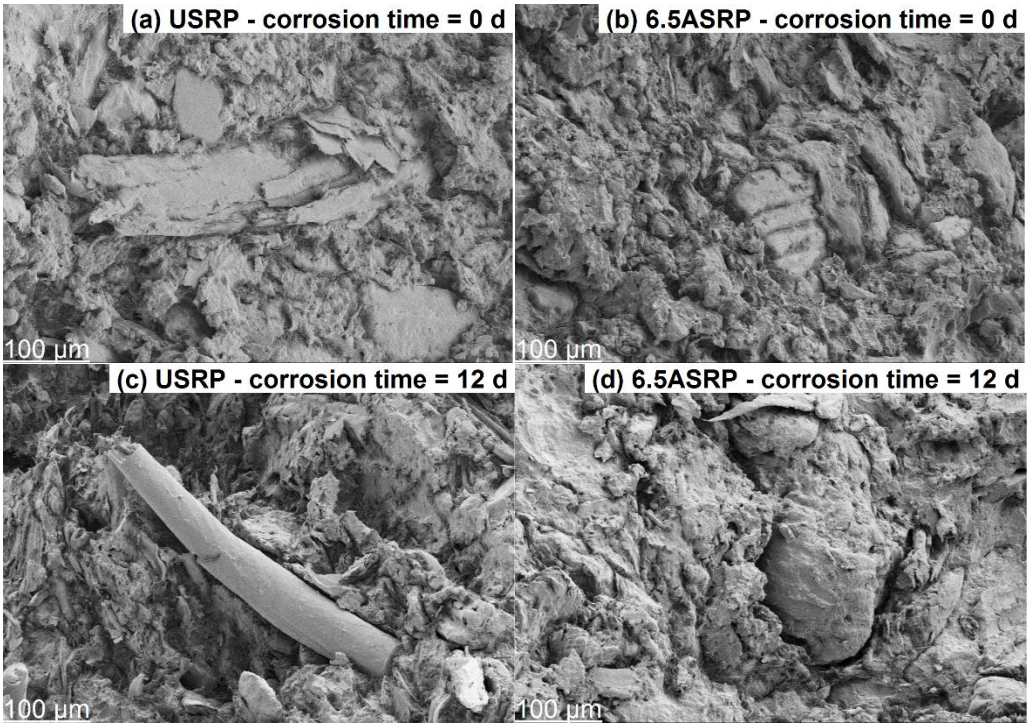

Fig. 5. SEM micrographs of the tensile fracture surfaces of the USRP and 6.5ASRP.

Fracture Surfaces Analysis of the SS/PVC Composites

The SEM micrographs of the tensile fracture surfaces of the USRP and representative ASRP with 6.5% NaOH are shown in Fig. 5. Figure 5(a) shows the control for comparison. In Fig. 5(b), most fibers were embedded in the matrix, and the part exposed on the surface had adhered to a small amount of matrix, indicating that good dispersion and compatibility between the fiber and matrix. Regardless of the fiber type, the fracture surfaces of USRP and 6.5ASRP after 12 d of corrosion formed clear boundaries between the fiber and matrix (Fig. 5(c) and (d)). Some fiber pull-outs and voids were also apparent on the fracture surfaces, which indicated the existence of micro-cracks and weak interfacial interaction. It is worth noting that the poor interfacial bonding led to stress that could not

be effectively transferred to the fiber from the matrix, resulting in fiber de-bonding and poor physico-mechanical properties.

Physico-mechanical Properties of the SS/PVC Composites

The physical-mechanical properties of the SS/PVC composites are shown in Fig. 6. It is clear that for the same corrosion cycle, irrespective of deviations, the average values of hardness as well as compressive, tensile, and flexural strengths followed the order: 4.5ASRP > 6.5ASRP > 2.5ASRP > 0.5ASRP > USRP. As expected, the alkali treatment noticeably improved the physico-mechanical properties of the composites because of the increased crystallinity and strength of the fiber and decreased hydrophilic character. Fibers with lower polarity are more compatible with the PVC matrix, resulting in a better dispersion of fibers in the matrix and improved wettability with the polymer. In other words, the physico-mechanical properties increased with increasing NaOH concentration up to 4.5%, and then slightly decreased at the higher NaOH concentration of 6.5%. The increase in the physico-mechanical properties is likely due to stronger fiber crystallinity, strength, and interfacial bonding, while the subsequent decrease in the physico-mechanical properties arose from weaker fiber crystallinity and strength due to strong alkali attack. Furthermore, the physico-mechanical properties exhibited a negative correlation with the corrosive cycle, as it caused deterioration of the interfacial bonding between the fiber and matrix, especially for samples with weaker initial interfacial bonding.

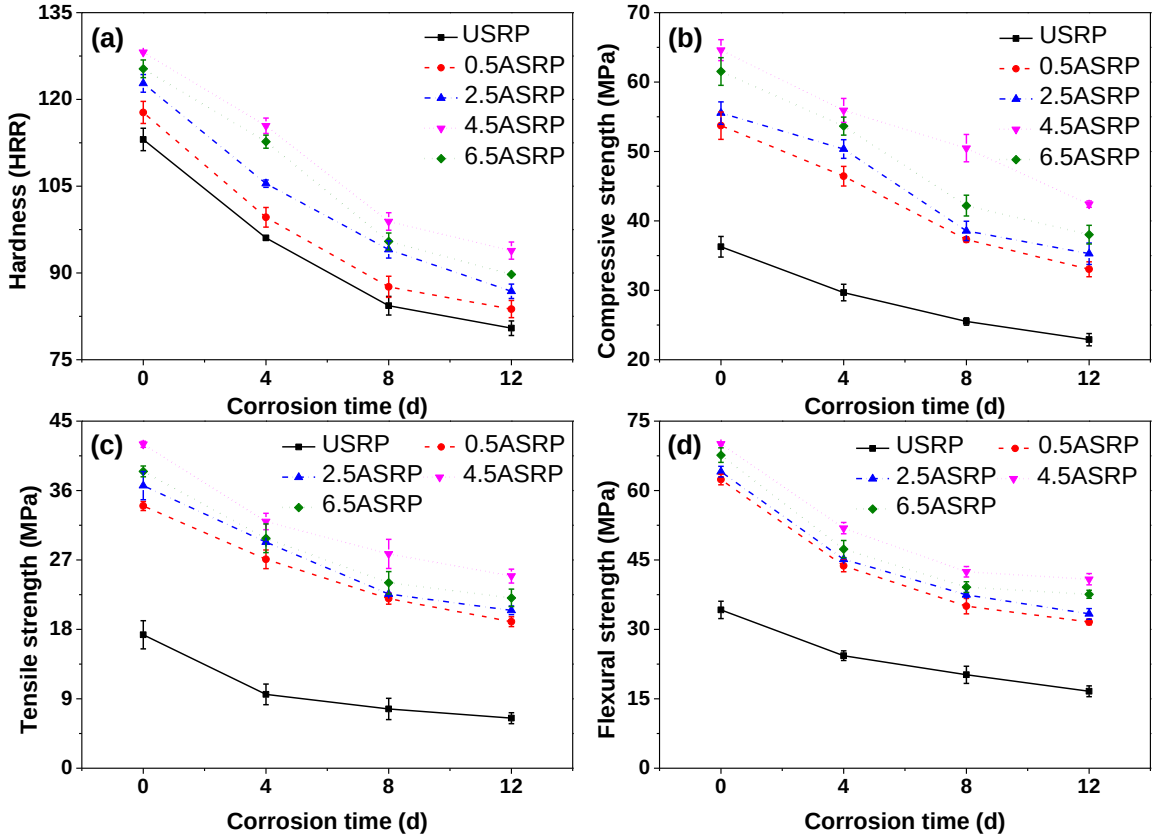

Fig. 6. Physico-mechanical properties of the SS/PVC composites

Friction and Wear Properties of the SS/PVC Composites

The friction coefficients and specific wear rates of the SS/PVC composites are shown in Fig. 7. Clearly, reinforcing the PVC matrix with alkali-treated SS fiber served to improve the wear resistance of the composites when compared with USRP. The wear resistance decreased in the following order: 4.5ASRP > 6.5ASRP > 2.5ASRP > 0.5ASRP > USRP.

In the case of 4.5ASRP, the μ and W_S values were lower than the other four materials at the same point in the corrosion cycle. This superior wear resistance can be attributed to the high crystallinity and strength of the SS fibers and to the strong interfacial bonding with PVC matrix achieved at a 4.5% NaOH concentration. This leads to stronger load-bearing fiber and requires more energy for de-bonding of fiber/matrix interface.

Upon further examination of Fig. 7, it can be seen that the SS/PVC composites exhibited a gradual rise in μ and W_S values with extended corrosion cycle. This is likely because the varying corrosive water bodies weakened the mechanical interlocking between the fiber and the matrix. In other words, the fibers received less support from the matrix, which lowered the wear resistance. Similar results have been reported in Jiang *et al.* (2017a, b). In addition, the wear debris of the pulled-out fibers, produced by de-bonding, participate in linear motion between the friction interfaces. This can result in the high resistance of relative motion and high removal of material.

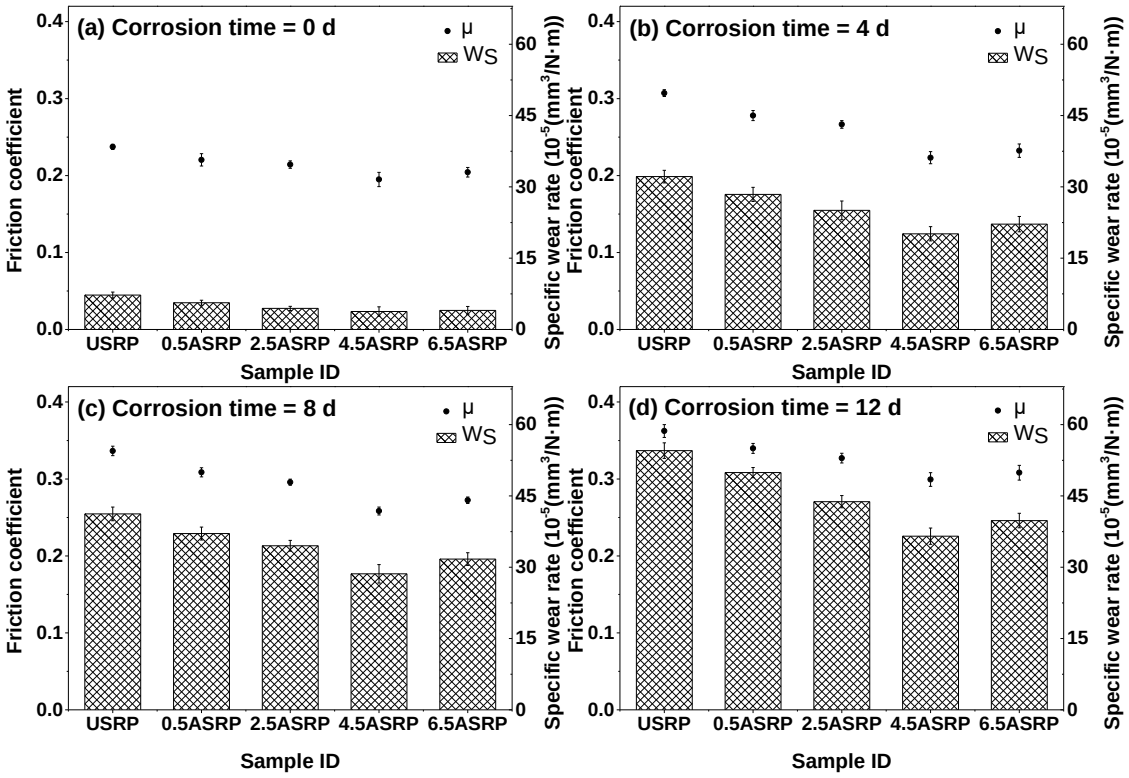

Fig. 7. Friction coefficients and specific wear rates of the SS/PVC composites

Thermogravimetric Analysis of the SS/PVC Composites

The dry sliding with high-velocity, high-load, and long-distance contributed to the high thermo-mechanical loading between the interacting surfaces of the counterpart and test sample, which caused increased temperatures. The high temperatures softened the

polymer matrix leading to poor interfacial bonding strength and subsequent high material removal. Thus, it is imperative to accurately evaluate the effect of varying corrosive water bodies on the pyrolysis behavior of the material to estimate the true wear rates. In the case of the SS/PVC composites (Fig. 8), there were two significant weight loss stages during the heating process. The first stage (250 to 350 °C) with a high weight loss was attributed to the thermal degradation of cellulose, hemicellulose, and lignin. Moreover, the HCl-elimination reaction of PVC takes place during this stage. The weight loss in the second stage (430 to 500 °C) was ascribed to the thermal degradation of the carbon chain of PVC, producing flammable volatiles.

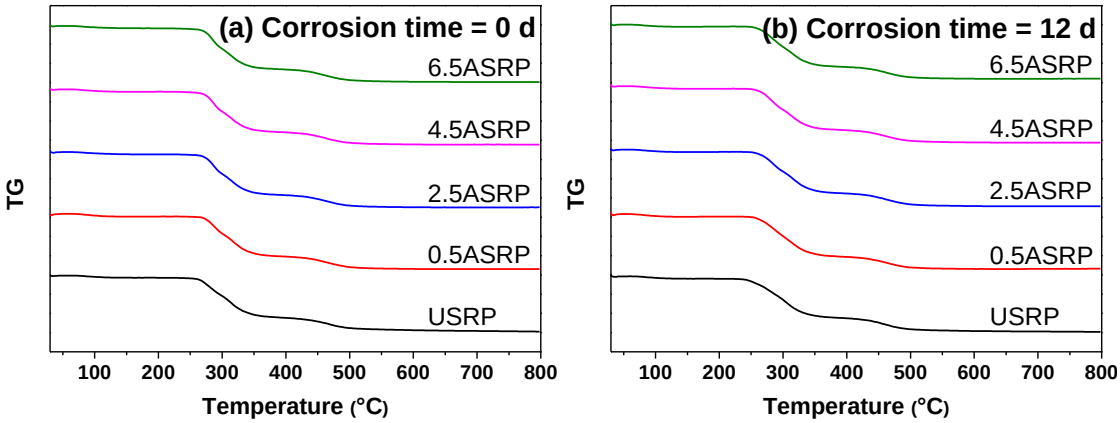

Fig. 8. TG curves of the SS/PVC composites

The pyrolysis temperature (T_P) of the SS/PVC composites was also calculated (Table 1). The results showed that the alkali-treated fibers improved the T_P of the PVC matrix.

Table 1. Pyrolysis Temperatures of the SS/PVC Composites

Sample ID	Corrosion Time (d)	Pyrolysis Temperature (°C)			
		First Stage		Second Stage	
		Onset	Termination	Onset	Termination
USRP	0	258.3	334.6	437.8	481.7
	12	250.2	326.6	430.7	473.9
0.5ASRP	0	268.6	335.4	437.5	486.4
	12	261.6	335.1	433.5	484.1
2.5ASRP	0	273.5	337.2	437.9	490.7
	12	262.6	335.5	435.1	485.2
4.5ASRP	0	273.7	342.7	439.5	491.3
	12	263.2	337.2	435.6	485.5
6.5ASRP	0	274.6	347.8	441.1	494.2
	12	264.6	339.3	437.9	489.4

The T_P values decreased in the following order: 6.5ASRP > 4.5ASRP > 2.5ASRP > 0.5ASRP > USRP. This is likely because the alkali-treated fibers were able to distribute into PVC more homogeneously than the untreated fibers, which absorb energy during heating resulting in less energy transmission to the PVC (Monteiro *et al.* 2012). This could strengthen the wear resistance of the SS/PVC composites in high temperature frictional environments. However, the SS/PVC composites had a decreasing trend of T_P as the corrosion cycles progressed. The polymer molecular chain becomes less stable when the

interfacial bonding strength between the fiber and matrix degrades as a result of the extended corrosion cycle. In sum, with lower strength interfacial bonding, heat resistance becomes weaker.

Wear Mechanisms of the SS/PVC Composites

The SEM micrographs of the worn surfaces of the USRP and representative ASRP with 4.5% NaOH are shown in Fig. 9. A close examination of Fig. 9 reveals evidence of abrasive wear on the worn surfaces after being subjected to 12 d of corrosion cycling. There were massive furrows on the worn surfaces, which could have been generated from the wear debris (that is, broken or pulled-out fibers) linear travel in relation to the sliding force. This result in agreement with the observation of Jiang *et al.* (2017a, b). The broken fiber debris was formed due to the brittleness of the third body (such as the micro-bulges on the counterface) generated during the sliding, which caused part of the fiber to chip off. The pulled-out fiber debris was formed by rapid degradation of interfacial bonding strength (that is, the grip strength of matrix to fiber), which failed to firmly hold the fibers resulting in rapid delamination. Previous studies have claimed that soft abrasive particles (such as plant fiber debris), clamped between the metal counterpart and the rigid wear component under high-speed movement at high temperatures and frictional loads, can also result in the formation of these features. These fiber molecules could bond together to form "incompressible lumps", which manifest as sharp-edged particles with high hardness (Zhang *et al.* 2016a,b; 2017). Wu *et al.* (2007) raised similar speculations in the wear study of metals by alfalfa powder. However, for the 4.5ASRP samples, the wear resistance was superior, as shown in the SEM micrograph in Fig. 9(b) when compared to Fig. 9(a).

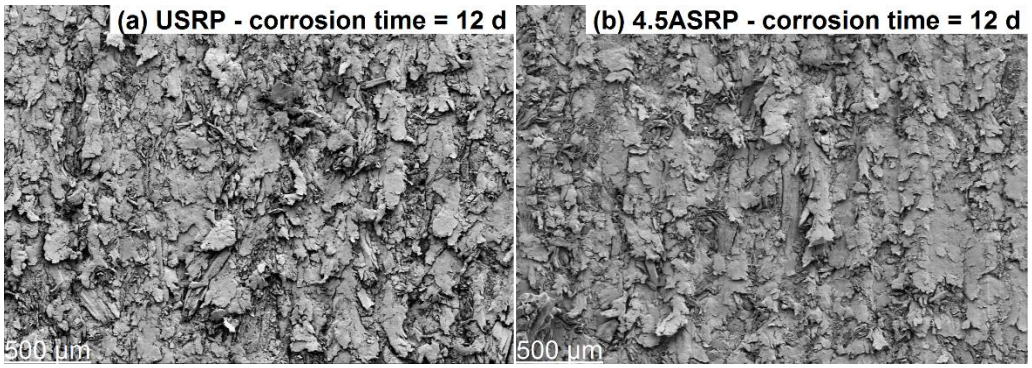

Fig. 9. SEM micrographs of the worn surfaces of the USRP and 4.5ASRP

CONCLUSIONS

1. Incorporation of alkali-treated SS fiber into the PVC matrix enhances the wear resistance of SS/PVC composites compared to the untreated SS fiber.
2. NaOH solution reacted with SS fibers and weakened the polarity and hydrophilicity of the resulting fiber, while yielding high crystallinity and improved mechanical properties. The 4.5% alkali-treated SS fiber endowed the SS/PVC composites with higher interfacial bonding and wear resistance compared with other alkali-treated SS fibers with different NaOH concentrations.
3. Exposure of the composites to extended simulated sea water and acid rain corrosion

cycle resulted in poor physical (including water repellency and hardness), mechanical, thermal, and wear-resistance properties. The predominant wear for SS/PVC composites after 12 d of corrosion cycling was abrasive wear associated with the formation of broken or pulled-out fibers.

ACKNOWLEDGEMENTS

This work was supported by the National Science and Technology Support Program (China), Grant. No. 2011BAD20B202-2.

REFERENCES CITED

Abdul, P. M., Jahim, J. M., Harun, S., Markom, M., Lutpi, N. A., Hassan, O., Balan, V., Dale, B. E., and Mohd Nor, M. T. (2016). "Effects of changes in chemical and structural characteristic of ammonia fibre expansion (AFEX) pretreated oil palm empty fruit bunch fibre on enzymatic saccharification and fermentability for biohydrogen," *Bioresource Technology* 211, 200-208. DOI: 10.1016/j.biortech.2016.02.135

Alawar, A., Hamed, A. M., and Al-Kaabi, K. (2009). "Characterization of treated date palm tree fiber as composite reinforcement," *Composites Part B: Engineering* 40(7), 601-606. DOI: 10.1016/j.compositesb.2009.04.018

Bajpai, P. K., Singh, I., and Madaan, J. (2013). "Tribological behavior of natural fiber reinforced PLA composites," *Wear* 297(1-2), 829-840. DOI: 10.1016/j.wear.2012.10.019

Cai, M., Takagi, H., Nakagaito, A. N., Katoh, M., Ueki, T., Waterhouse, G. I. N., and Li, Y. (2015). "Influence of alkali treatment on internal microstructure and tensile properties of abaca fibers," *Industrial Crops and Products* 65, 27-35. DOI: 10.1016/j.indcrop.2014.11.048

Cai, M., Takagi, H., Nakagaito, A. N., Li, Y., and Waterhouse, G. I. N. (2016). "Effect of alkali treatment on interfacial bonding in abaca fiber-reinforced composites," *Composites Part A: Applied Science and Manufacturing* 90, 589-597. DOI: 10.1016/j.compositesa.2016.08.025

Chand, N., and Dwivedi, U. K. (2006). "Effect of coupling agent on abrasive wear behaviour of chopped jute fibre-reinforced polypropylene composites," *Wear* 261(10), 1057-1063. DOI: 10.1016/j.wear.2006.01.039

Chand, N., and Dwivedi, U. K. (2010). "Sliding wear and friction characteristics of sisal fibre reinforced polyester composites: Effect of silane coupling agent and applied load," *Polymer Composites* 29(3), 280-284. DOI: 10.1002/pc.20368

Chin, C. W., and Yousif, B. F. (2009). "Potential of kenaf fibres as reinforcement for tribological applications," *Wear* 267(9-10), 1550-1557. DOI: 10.1016/j.wear.2009.06.002

El-Tayeb, N. S. M. (2008). "A study on the potential of sugarcane fibers/polyester composite for tribological applications," *Wear* 265(1-2), 223-235. DOI: 10.1016/j.wear.2007.10.006

Friedrich, D., and Luible, A. (2016). Investigations on ageing of wood-plastic composites for outdoor applications: A meta-analysis using empiric data derived from diverse

weathering trials," *Construction and Building Materials* 124, 1142-1152. DOI: 10.1016/j.conbuildmat.2016.08.123

GB/T 35378 (2017). "Testing methods for tensile mechanical properties of plant short individual fibers," National Standardization Administration of People's Republic of China, Beijing, China.

GB/T 17657 (2013). "Test methods of evaluating the properties of wood–based panels and surface decorated wood–based panels," National Standardization Administration of People's Republic of China, Beijing, China.

GB/T 20312 (2006). "Hygrothermal performance of building materials and products - Determination of hygroscopic sorption properties," National Standardization Administration of People's Republic of China, Beijing, China.

GB/T 3398.1 (2008). "Plastic - Determination of hardness," National Standardization Administration of People's Republic of China, Beijing, China.

GB/T 1041 (1992). "Plastic - Determination of compressive properties," National Standardization Administration of People's Republic of China, Beijing, China.

GB/T 1040.1 (2006). "Plastic - Determination of tensile properties," National Standardization Administration of People's Republic of China, Beijing, China.

GB/T 9341 (2008). "Plastic - Determination of flexural properties," National Standardization Administration of People's Republic of China, Beijing, China.

Hashmi, S. A. R., Dwivedi, U. K., and Chand, N. (2007). "Graphite modified cotton fibre reinforced polyester composites under sliding wear conditions," *Wear* 262(11-12), 1426-1432. DOI: 10.1016/j.wear.2007.01.014

Jeamtrakull, S., Kositchaiyong, A., Markpin, T., Rosarpitak, V., and Sombatsompop, N. (2012). "Effects of wood constituents and content, and glass fiber reinforcement on wear behavior of wood/PVC composites," *Composites Part B: Engineering* 43(7), 2721-2729. DOI: 10.1016/j.compositesb.2012.04.031

Jiang, L., He, C., Fu, J., and Chen, D. (2017a). "Wear behavior of straw fiber-reinforced polyvinyl chloride composites under simulated acid rain conditions," *Polymer Testing* 62, 373-381. DOI: 10.1016/j.polymertesting.2017.07.028

Jiang, L., He, C., Fu, J., and Chen, D. (2017b). "Wear behavior of wood-plastic composites in alternate simulated sea water and acid rain corrosion conditions," *Polymer Testing* 63, 236-243. DOI: 10.1016/j.polymertesting.2017.08.031

Krishnaiah, P., Ratnam, C. T., and Manickam, S. (2017). "Enhancements in crystallinity, thermal stability, tensile modulus and strength of sisal fibres and their PP composites induced by the synergistic effects of alkali and high intensity ultrasound (HIU) treatments," *Ultrasonics Sonochemistry* 34, 729-742. DOI: 10.1016/j.ultsonch.2016.07.008

Matuana, L. M., Jin, S., and Stark, N. M. (2011). "Ultraviolet weathering of HDPE/wood-flour composites coextruded with a clear HDPE cap layer," *Polymer Degradation and Stability* 96(1), 97-106. DOI: 10.1016/j.polymdegradstab.2010.10.003

Monteiro, S. N., Calado, V., Rodriguez, R. J. S., and Margem, F. M. (2012). "Thermogravimetric behavior of natural fibers reinforced polymer composites—An overview," *Materials Science and Engineering: A* 557, 17-28. DOI: 10.1016/j.msea.2012.05.109

Nirmal, U., Yousif, B. F., Rilling, D., and Brevern, P. V. (2010). "Effect of betelnut fibres treatment and contact conditions on adhesive wear and frictional performance of polyester composites," *Wear* 268(11-12), 1354-1370. DOI:

10.1016/j.wear.2010.02.004
Nirmal, U., Hashim, J., and Low, K. O. (2012). "Adhesive wear and frictional performance of bamboo fibres reinforced epoxy composite," *Tribology International* 47, 122-133. DOI: 10.1016/j.triboint.2011.10.012
Oudiani, A. E., Chaabouni, Y., Msahli, S., and Sakli, F. (2011). "Crystal transition from cellulose I to cellulose II in NaOH treated *Agave americana L.* fibre," *Carbohydrate Polymers* 86(3), 1221-1229. DOI: 10.1016/j.carbpol.2011.06.037
Oushabi, A., Sair. S., Hassani. F. O., Abboud. Y., Tanane. O., and Bouari. A. E. (2017). "The effect of alkali treatment on mechanical, morphological and thermal properties of date palm fibers (DPFs): Study of the interface of DPF–Polyurethane composite," *South African Journal of Chemical Engineering* 23, 116-123. DOI: 10.1016/j.sajce.2017.04.005
Phuong, N. T., Sollogoub, C., and Guinault, A. (2010). "Relationship between fiber chemical treatment and properties of recycled pp/bamboo fiber composites," *Journal of Reinforced Plastics and Composites* 29(21), 3244-3256. DOI: 10.1177/0731684410370905
Saha, P., Manna, S., Chowdhury, S. R., Sen, R., Roy, D., and Adhikari, B. (2010). "Enhancement of tensile strength of lignocellulosic jute fibers by alkali-steam treatment," *Bioresource Technology* 101(9), 3182-3187. DOI: 10.1016/j.biortech.2009.12.010
Shalwan, A., and Yousif, B. F. (2013). "In state of art: Mechanical and tribological behaviour of polymeric composites based on natural fibres," *Materials & Design* 48(2), 14-24. DOI: 10.1016/j.matdes.2012.07.014
Singh Gill, N., and Yousif, B. F. (2009). "Wear and frictional performance of betelnut fibre-reinforced polyester composite," *Proceedings of the Institution of Mechanical Engineers, Part J: Journal of Engineering Tribology* 223(2), 183-194. DOI: 10.1243/13506501JET516
Wu, J., Huang, J., Zhang, W., and Zhao, W. (2007). "Friction and wear behavior of the metals by alfalfa powder," *Tribology* 27(1), 88-90. DOI: 10.3321/j.issn:1004-0595.2007.01.019
Xin, X., Xu, C. G., and Qing, L. F. (2007). "Friction properties of sisal fibre reinforced resin brake composites," *Wear* 262(5-6), 736-741. DOI: 10.1016/j.wear.2006.08.010
Yang, T. H., Yang, T. H., Chao, W. C., and Leu, S.Y. (2015). "Characterization of the property changes of extruded wood-plastic composites during year round subtropical weathering," *Construction and Building Materials* 88, 159-168. DOI: 10.1016/j.conbuildmat.2015.04.019
Yousif, B. F., and El-Tayeb, N. S. M. (2008). "Adhesive wear performance of T-OPRP and UT-OPRP composites," *Tribology Letters* 32(3), 199-208. DOI: 10.1007/s11249-008-9381-7
Yousif, B. F., Lau, S. T. W., and McWilliam, S. (2010a). "Polyester composite based on betelnut fibre for tribological applications," *Tribology International* 43(1-2), 503-511. DOI: 10.1016/j.triboint.2009.08.006
Yousif, B. F., Leong, O. B., Ong, L. K., and Jye, W. K. (2010b). "The effect of treatment on tribo-performance of CFRP composites," *Recent Patents on Materials Science* 2(1), 67-74. DOI: 10.2174/1874465610902010067
Yousif, B. F., and Nirmal, U. (2011). "Wear and frictional performance of polymeric composites aged in various solutions," *Wear* 272(1), 97-104. DOI: 10.1016/j.wear.2011.07.006

Zhang, K., Jiang, L., and Huang, X. (2016a). "Heat treatment process optimization of roller material of wheat mill against abrasive wear," *Transactions of the Chinese Society of Agricultural Engineering* 32(21), 271-276. DOI: 10.11975/j.issn.1002-6819.2016.21.037.

Zhang, K., Jiang, L., and Wang, J. (2016b). "Wheat powder abrasion wear resistance of white cast iron with different chromium content," *Materials for Mechanical Engineering* 40(12), 57-60. DOI: 10.11973/jxgccl201612013

Zhang, K., Jiang, L., and Yao, Y. (2017). "Experiment of white iron abrasive wear for wheat grain powder," *Journal of the Chinese Cereals and Oils Association* 32(1), 109-112. DOI: 10.3969/j.issn.1003-0174.2017.01.019.

Article submitted: January 4, 2018; Peer review completed: February 26, 2018; Revised version received: March 3, 2018; Accepted: March 12, 2018; Published: March 15, 2018.
DOI: 10.15376/biores.13.2.3362-3376